

# The $^{10}\text{Li}$ spectrum and the $^{11}\text{Li}$ properties

E. Garrido

*Instituto de Estructura de la Materia, CSIC, Serrano 123, E-28006 Madrid, Spain*

D.V. Fedorov and A.S. Jensen

*Institute of Physics and Astronomy, University of Aarhus, DK-8000 Aarhus C, Denmark*

---

## Abstract

The neutron- $^9\text{Li}$  interaction and the corresponding low-energy  $^{10}\text{Li}$  spectrum are decisive for the properties of  $^{11}\text{Li}$  described as a three-body system ( $n+n+^9\text{Li}$ ). We compute structure and breakup properties of  $^{11}\text{Li}$  as function of this interaction. The hyperfine structure due to the spin  $3/2$  of both  $^9\text{Li}$  and  $^{11}\text{Li}$  is needed and treated with special care. We use the hyperspherical adiabatic expansion of the Faddeev equations for the structure and the participant-spectator model for the breakup reactions of  $^{11}\text{Li}$ . We use established experimental constraints of both  $^{11}\text{Li}$  (binding energy, size and differential breakup cross sections) and of  $^{10}\text{Li}$  (a virtual  $s$ -state below 50 keV and a  $p$ -resonance around 0.54 MeV)<sup>1</sup>. Another  $p$ -resonance must then be present below 0.54 MeV and another  $s$ -level must be present between about 0.5 MeV and 1 MeV depending on unknown spin assignments. All established facts are in agreement with our predictions obtained within the same consistent model.

---

*PACS:* 21.45.+v, 25.10.+s, 25.60.-t, 25.60.Gc

## 1 Introduction and motivation

The  $^{11}\text{Li}$  nucleus is a prominent example of the so-called Borromean nuclei which can be described as a three-body system ( $^9\text{Li}$  plus two neutrons) where none of the internal two-body subsystems is bound [1]. Few-body models

---

<sup>1</sup> Bound and virtual states have positive and negative imaginary wave numbers, respectively (zero real parts). Thus the virtual  $s$ -state energies should strictly speaking be negative, but we shall here and throughout the paper omit the minus sign and use the absolute value.

and techniques have been very successful [2] but they must necessarily rely heavily on the underlying two-body interactions. Phenomenological interaction parameters for the neutron- $^9\text{Li}$  system have usually been obtained by constraints of the properties of  $^{11}\text{Li}$ . However, comparison between measurements and these theories suffered from the fact that essentially all theoretical investigations assumed spin zero for both  $^9\text{Li}$  and  $^{11}\text{Li}$ . This is very unsatisfactory and also rather surprising especially considering the huge amounts of work invested in  $^{11}\text{Li}$ . Substantially more complicated models are required but the available techniques are also very developed. The new experimental results have prompted us to reinvestigate the present  $^{10}\text{Li}$ - $^{11}\text{Li}$  connection.

### 1.1 *The two-body system*

The experimental data about the properties of  $^{10}\text{Li}$ , and therefore also of  $^{11}\text{Li}$ , still remain incomplete. The quantum numbers of the  $^{10}\text{Li}$  ground state are not firmly established. The first attempt to measure the  $^{10}\text{Li}$  spectrum was made by Wilcox et al. [3] placing the ground state of the unbound nucleus  $^{10}\text{Li}$  at  $0.80\pm 0.25$  MeV. More recent experiments [4] concluded the existence of a very low-lying state in  $^{10}\text{Li}$ , although its quantum numbers were not determined. In [5] the authors identified the  $1^+$ -state as the most probable  $^{10}\text{Li}$  ground state. This parity inversion was already discussed much earlier for neighboring nuclei in [6] and for  $^{10}\text{Li}$  in [7].

A probable  $s$ -state as ground state of  $^{10}\text{Li}$  was experimentally suggested in [8]. In [9] a  $p$ -resonance was observed at an energy of  $538\pm 62$  keV, together with a weak evidence of a barely unbound  $s$  or  $p$ -resonance in  $^{10}\text{Li}$ . A bit later, Abramovich et al. [10] and Zinser et al. [11] claimed that the ground state of  $^{10}\text{Li}$  corresponds to a very low lying  $l=0$  state. In the first case the energies of the doublet  $2^-/1^-$  were given to be 27 keV and 88 keV, respectively, while in [11] the energy of the low-lying  $s$ -state was established to be below 50 keV.

Recent experiments have been performed in order to clarify this puzzle. In [12] the existence of a  $p$ -resonance, probably the  $2^+$  state, at  $0.54\pm 0.06$  MeV has been confirmed, and the existence of a lower  $p$ -resonance, the  $1^+$  state, has been found at  $0.24\pm 0.06$  MeV. Although the existence of a low-lying  $s$ -state is not confirmed in this work, they emphasize that part of the observed strength at the threshold might represent  $l=0$  strength.

More recently, Thoennessen et al. [13] have repeated the experiment of Kryger et al. [8] with improved energy resolution in order to establish more stringent limits of the  $s$ -wave parameters. They concluded that a low-lying  $s$ -state was observed with a scattering length of at least 20 fm corresponding to a peak energy of less than 50 keV. They also found indications of a  $p$ -state around

540 keV, and they did not rule out another  $p$ -state at  $\sim 240$  keV.

In [14] the experimental spectrum was fitted with a  $p$ -state at  $500 \pm 60$  keV and width  $400 \pm 60$  keV. Substitution of this resonance by combination of one  $s$  and one  $p$  or combination of two  $p$ 's provided fits which were less significant due to the increase of fit parameters. Inclusion of the extra  $s$ -wave or  $p$ -wave moved the 500 keV state up by 15 and 25 keV, respectively. No other states were identified, either because they were not populated, or because the experimental resolution was insufficient. Although there is no evidence for a state at  $\sim 250$  keV there is a small enhancement, also seen in [9].

Finally the last experiment by Chartier et al. [15] produced  $^{10}\text{Li}$  by proton knockout of  $^{11}\text{Be}$ . The measured resulting  $^9\text{Li}$  nucleus in the ground state is predominantly produced from  $s$ -wave neutron emission of  $^{10}\text{Li}$  which is concluded to resemble the neutron configuration in the  $^{11}\text{Be}$  ground state. Thus the ground state of the  $n$ - $^9\text{Li}$  system is an  $s$ -wave below 50 keV.

As a consequence of all this it is well established experimentally that the ground state of  $^{10}\text{Li}$  corresponds to a very low-lying  $s$ -state. Furthermore a  $p$ -resonance at an energy of around 0.5 MeV is present in the  $^{10}\text{Li}$  spectrum. The other quantum numbers specifying the couplings of these states remain so far unknown. Also the presence of a second  $p$ -resonance at around 0.25 MeV is not well established and another  $s$ -state, which necessarily also must be present in the low energy spectrum, is entirely unknown.

The observed resonances or virtual states in the neutron- $^9\text{Li}$  spectrum are related to the second  $s_{1/2}$  and the first  $p_{1/2}$ -states. The first  $s_{1/2}$  and the lowest  $p_{3/2}$ -states are occupied in the  $^9\text{Li}$ -nucleus. The lowest  $s_{1/2}$ -state is strongly bound and the energy of the  $p_{3/2}$ -state can be estimated as the one-neutron separation energy of  $^9\text{Li}$ , i.e. 4.1 MeV [16,17]. Strictly speaking this energy applies to  $^9\text{Li}$  whereas both the  $p_{3/2}$  and  $p_{1/2}$ -states discussed in the present context are related to the  $^{10}\text{Li}$ -system.

From the theoretical side, initial calculations [18] considered the ground state of  $^{10}\text{Li}$  to be the  $1^+$  state at an energy of 810 keV, as given in [3]. However in [18] is already mentioned the possibility that the ground state of  $^{10}\text{Li}$  is  $2^-$ , as discussed in [7]. The first three-body computation of the  $^{11}\text{Li}$  properties [19] predicted that, to be consistent with the available data,  $^{10}\text{Li}$  should have an  $s$ -state below 300 keV in conflict with the 800 keV at that time believed to be the ground state resonance energy.

In [20] it was confirmed that core momentum distributions after fragmentation of  $^{11}\text{Li}$  were consistent with a low lying  $s$ -state in  $^{10}\text{Li}$ , and it was estimated that  $^{11}\text{Li}$  has nearly 50% of  $s$ -wave motion between one neutron and the core. This fact of a negative parity state was contradicted by subsequent microscopic calculations [21,22] that predicted a  $1^+$  assignment for the ground state of  $^{10}\text{Li}$ .

On the other hand, in [23,24] an  $s$ -state was predicted to be the ground state of  $^{10}\text{Li}$ .

## 1.2 The three-body system

In [2,25] a method to solve Faddeev equations in coordinate space is developed in detail. This method is especially suitable to describe the large distance behavior of weakly bound three-body systems. In [26,27] we have shown that combination of this method to describe  $^{11}\text{Li}$  and the simple sudden approximation as fragmentation reaction model are sufficient to reproduce the shape of the experimental neutron and core momentum distributions after fast fragmentation of  $^{11}\text{Li}$  on a light target. We have shown that the agreement with the experiment is obtained only when the final interaction between fragments is included, and also when a low-lying  $s$ -state is present in  $^{10}\text{Li}$ . Inclusion of only  $p$ -states in the  $^{10}\text{Li}$  spectrum necessarily leads to too broad neutron momentum distributions.

In [28] we have investigated the angular correlations after breakup of  $^6\text{He}$  and  $^{11}\text{Li}$ , and we have shown that the presence of a low lying  $s$ -state gives rise to a very different angular distribution compared to nuclei as  $^6\text{He}$  where the  $p$ -resonances dominate in the neutron-core system. The experimental data for the angular distribution arising from  $^{11}\text{Li}$  was later published [29] and found to be in agreement with the distribution predicted in [28]. This is imperative evidence of strong  $s$ -wave configurations in both  $^{10}\text{Li}$  and  $^{11}\text{Li}$ .

More detailed calculations of momentum distributions after fragmentation of  $^{11}\text{Li}$  on light targets are reported in [30]. The agreement with the experiments is found to be rather good when around 40% of  $p$ -wave is present in the relative neutron- $^9\text{Li}$  motion. Nevertheless the precise energies and quantum numbers of the  $^{10}\text{Li}$  states are not well established, since the momentum distributions are mainly sensitive to the average energies of the doublets  $1^-/2^-$  and  $1^+/2^+$  [27]. For  $^{10}\text{Li}$  these states arise from couplings of the  $^9\text{Li}$ -spin of  $3/2$  to the available  $s_{1/2}$  and  $p_{1/2}$  neutron states. In  $^{11}\text{Li}$  the Pauli principle prevents the neutrons from both choosing the lowest state. Parity then requires an equal distribution within each doublet. Thus, most observables are not sensitive to the precise positions of these doublets, only to their average values. This is the reason why so many theoretical computations agree fairly well with experiments even with the obviously wrong assumptions of spin zero for both  $^9\text{Li}$  and  $^{11}\text{Li}$ . The invariant mass spectrum is an exception which could be sensitive to the precise position of the resonances and virtual states.

Very recently the fragmentation model used in [30] has been implemented to take into account the interaction between each of the halo constituents and the

target, as well as to include Coulomb interaction, making the method valid not only for light targets, but also for intermediate and heavy targets. This is the participant–spectator method described in details in [31]. The method works well for  ${}^6\text{He}$ , where essentially no uncertainties in the neutron–core interaction are present.

This success for the case of  ${}^6\text{He}$  leads us to turn the problem around and investigate in details which structure of  ${}^{10}\text{Li}$  is consistent with the firmly established properties of both  ${}^9\text{Li}$ ,  ${}^{10}\text{Li}$  and  ${}^{11}\text{Li}$ . First the neutron- ${}^9\text{Li}$  potential must be consistent with the structure of  ${}^9\text{Li}$  and the energies and quantum numbers of the established two-body resonances and virtual states must be reproduced. Then also the known  ${}^{11}\text{Li}$  three-body structure must be reproduced. The unavoidable facts are one and only one particle bound state with angular momentum and parity  $\frac{3}{2}^-$ , with binding of  $295\pm 35$  keV [32], with large interaction cross sections on all targets and with narrow fragment momentum distributions after breakup. The complicated model with finite core spin is then inescapable.

### 1.3 Model dependence

The measured differential or total  ${}^{11}\text{Li}$  reaction cross sections are interpreted as evidence for an exceptionally large spatial extension of the neutron matter and a correlated wave function mixing roughly equally relative neutron-core  $s$  and  $p$ -states. The quantitative details must necessarily be extracted by use of model computations. Apart from the binding energy of about 0.30 MeV the crucial parameter is the  $p$ -wave content determined to be about 40% in a rather successful model [30,31], which is able to describe essentially all measured breakup cross sections. The breakup cross sections are first of all sensitive to this  $s$ -wave content and we shall therefore aim at reproducing these 60% in the  ${}^{11}\text{Li}$  structure.

The model dependence of the extracted results has to be minimized as far as possible. This important issue can be illustrated by two different examples. The first is the interpretation of the neutron momentum distribution observed in breakup reactions. Narrower distributions result from inclusion of both final state interactions and from removal of those parts of the three-body wave function where only one or two of the three halo particles appear after the reaction, i.e. true three-body breakup [30,31]. A larger fraction of neutron-core  $s$ -wave would compensate and delusively reproduce the measurement.

The second example is the interaction cross section often attempted to be expressed in terms of a corresponding value of the  ${}^{11}\text{Li}$  root mean square radius. This interpretation is also model dependent as evidenced by the different re-

sults, i.e. radii of  $3.1\pm 0.3$  fm [33],  $3.53\pm 0.10$  fm [34] and  $3.62\pm 0.19$  fm [35] from Glauber models with parametrized densities, three-body densities and from elastic proton scattering with gaussian densities, respectively.

The first of these, off hand least sophisticated, analyses [33] used parametrized static densities of various kinds. The second analysis used a reaction model accounting for the few-body correlations obviously present in the initial wave function [34]. The essential input is then the three-body ground state wave function and the resulting radius relies heavily on the properties of this choice. The result of about 3.53 fm quoted above arises from two-body interactions where the virtual states and resonances cannot all agree with the established experimental information. Their average positions are unrealistically low and there is no spin splitting in the calculation. The  $p$ -wave content is almost 60% and the presently accepted use of a three-body interaction for fine tuning is not applied. The third analysis is from elastic proton scattering resulting in an even larger radius [35]. Again this is one numerical value and corresponding results for  ${}^6\text{He}$  are in conflict with other information.

Avoiding the model dependence entirely is not possible. Minimizing the uncertainties at least require that all effects influencing the observables in question must be accounted for in the model. The safest is to use one consistent model with all anticipated physical effects included and with one set of parameters reproducing all measured data from the two-body input data to the differential breakup cross sections. We rely on the three-body structure model [2] and the reaction models developed for systems precisely like  ${}^{11}\text{Li}$  [30,31].

The paper is organized as follows: In section 2 we briefly sketch the method used to construct the three-body wave function and the model to compute the breakup cross sections. We continue in section 3 with the details of the interactions involved in the particular case of  ${}^{11}\text{Li}$ . In section 4 we show results for the  ${}^{11}\text{Li}$  wave function and for different relevant observables after fragmentation reactions. Finally section 5 contains the summary and the conclusions.

## 2 Method

The wave function of the three-body halo system is obtained by solving the Faddeev equations in coordinate space [2,25]. This is done by writing each of the three Faddeev equations in terms of each of the three sets of hyperspherical coordinates  $(\rho, \Omega_i)$ ,  $\Omega_i = (\alpha_i, \Omega_{x_i}, \Omega_{y_i})$ , where the index  $i$  is related to a given Jacobi system. The three-body wave function  $\Psi^{(JM)}$  is then a sum of the three Faddeev components, each of them expanded for a given  $\rho$  in terms of

a complete sets of generalized angular functions  $\Phi_n^{(i)}(\rho, \Omega_i)$

$$\Psi^{(JM)} = \frac{1}{\rho^{5/2}} \sum_n f_n(\rho) \sum_{i=1}^3 \Phi_n^{(i)}(\rho, \Omega_i) . \quad (1)$$

The angular wave functions are solutions of the angular part of the Faddeev equations

$$\frac{\hbar^2}{2m} \frac{1}{\rho^2} \hat{\Lambda}^2 \Phi_n^{(i)} + V_{jk}(\Phi_n^{(i)} + \Phi_n^{(j)} + \Phi_n^{(k)}) \equiv \frac{\hbar^2}{2m} \frac{1}{\rho^2} \lambda_n(\rho) \Phi_n^{(i)} , \quad (2)$$

where  $\{i, j, k\}$  is a cyclic permutation of  $\{1, 2, 3\}$ ,  $m$  is a normalization mass,  $V_{jk}$  is the two-body interaction between particles  $j$  and  $k$  and  $\hat{\Lambda}^2$  is the  $\rho$ -independent part of the kinetic energy operator. The expression for  $\hat{\Lambda}^2$  is given in [2,25].

The radial functions  $f_n(\rho)$  are the solutions of the coupled set of “radial” differential equations

$$\begin{aligned} \left( -\frac{d^2}{d\rho^2} - \frac{2m(E - V_3(\rho))}{\hbar^2} + \frac{\lambda_n(\rho)}{\rho^2} + \frac{15}{4\rho^2} - Q_{nn} \right) f_n(\rho) \\ = \sum_{n' \neq n} \left( 2P_{nn'} \frac{d}{d\rho} + Q_{nn'} \right) f_{n'}(\rho) , \end{aligned} \quad (3)$$

where  $V_3$  is an anticipated three-body potential and the eigenvalues of the angular part,  $\lambda_n(\rho)$ , enter as effective potentials. The functions  $P$  and  $Q$  are defined as the angular integrals

$$P_{nn'}(\rho) \equiv \sum_{i,j=1}^3 \int d\Omega \Phi_n^{(i)*}(\rho, \Omega) \frac{\partial}{\partial \rho} \Phi_{n'}^{(j)}(\rho, \Omega) , \quad (4)$$

$$Q_{nn'}(\rho) \equiv \sum_{i,j=1}^3 \int d\Omega \Phi_n^{(i)*}(\rho, \Omega) \frac{\partial^2}{\partial \rho^2} \Phi_{n'}^{(j)}(\rho, \Omega) . \quad (5)$$

The observables obtained after fragmentation of  $^{11}\text{Li}$  are computed by using the participant–spectator method [31]. The breakup cross sections are obtained by adding the incoherent contributions from processes where one, two, or three halo particles simultaneously interact with the target. The interaction with the target of one of them (participant) is described by a phenomenological optical potential and the black disk model is used for the other two particles (spectators).

Let us assume that the halo constituent  $i$  is the participant and the final state can be described as two independent two-body systems, one made by particle  $i$  and the target 0, and the second made by the remaining halo constituents  $j$  and  $k$ . This final state description is appropriate for large momentum transfer processes in which the constituent  $i$  is violently removed from the projectile. Under these assumptions, and working in the frame of the halo projectile, the differential cross sections can be written as [30,31]

$$\frac{d^9\sigma_{el}^{(i)}(\mathbf{P}', \mathbf{p}'_{jk}, \mathbf{q})}{d\mathbf{P}' d\mathbf{p}'_{jk} d\mathbf{q}} = \frac{d^3\sigma_{el}^{(0i)}(\mathbf{p}_{0i} \rightarrow \mathbf{p}'_{0i})}{d\mathbf{q}} \frac{P_{dis}(\mathbf{q})}{2J+1} \sum_{Ms'_{jk}\Sigma'_{jk}\Sigma'_i} |M_{s'_{jk}\Sigma'_{jk}\Sigma'_i}^{(JM)}|^2, \quad (6)$$

$$\frac{d^6\sigma_{abs}^{(i)}(\mathbf{P}', \mathbf{p}'_{jk})}{d\mathbf{P}' d\mathbf{p}'_{jk}} = \sigma_{abs}^{(0i)}(p_{0i}) \frac{1}{2J+1} \sum_{Ms'_{jk}\Sigma'_{jk}\Sigma'_i} |M_{s'_{jk}\Sigma'_{jk}\Sigma'_i}^{(JM)}|^2. \quad (7)$$

where eq.(6) and (7) refer to the cases in which  $i$  is elastically scattered and absorbed by the target, respectively. The cross sections  $d^3\sigma_{el}^{(0i)}/d\mathbf{q}$  and  $\sigma_{abs}^{(0i)}$  are the differential elastic and absorption cross sections for the participant–target scattering. The momenta  $\mathbf{P}'$ ,  $\mathbf{p}'_{jk}$ , and  $\mathbf{p}'_{0i}$  are the relative momenta in the final state between the center of mass of the two final two-body systems, between the halo constituents  $j$  and  $k$ , and between  $i$  and the target, respectively. The momentum  $\mathbf{q}$  is the momentum transfer in the process. The quantum numbers  $(J, M)$  are the total spin and its third component of the halo nucleus,  $(s'_{jk}, \Sigma'_{jk})$  are the spin and third component of the two-body final state made by particles  $j$  and  $k$ , and  $\Sigma'_i$  is the final state third component of the spin of particle  $i$ . The target is assumed to have spin zero.

The expressions are then correct when the participant  $i$  has spin 0 or 1/2, but we shall employ them even for the spin of 3/2 corresponding to the  $^9\text{Li}$ -core. We expect this is a very accurate approximation. The function  $P_{dis}(\mathbf{q})$  in eq.(6) is included to remove the non-zero component of the three-body bound state plus target in the final state, that represents elastic scattering of the halo nucleus as a whole. Finally,  $M_{s'_{jk}\Sigma'_{jk}\Sigma'_i}^{(JM)}$  is the overlap between the  $jk$ -wave function in the final state and the wave function of the three-body projectile.

In [31] all the details about the participant–spectator model are given, as well as the optical potentials used to describe the interaction between participant  $i$  and the target.



### 3 Two-body interactions and $^{11}\text{Li}$ wave function

To obtain the  $^{11}\text{Li}$  wave function by use of the procedure sketched above one needs to specify the two-body interactions entering in eq.(2), i.e. the neutron-neutron and the neutron- $^9\text{Li}$  interactions.

The neutron-neutron interaction is specified in [36]. The neutron- $^9\text{Li}$  interaction is obviously decisive in order to establish the  $^{10}\text{Li}$  spectrum. We therefore must be very careful in the choices of both form and parameters. Results from previous work cannot be used directly since we want, and perhaps even need, a better correspondence between core-density and potentials of both core and valence neutrons.

We begin with the core density and potential of the core neutrons. The  $^9\text{Li}$ -core consists of two neutrons and two protons in the  $s_{1/2}$ -shell and four neutrons and one proton in the  $p_{3/2}$ -shell. The mean square radius of  $^9\text{Li}$  is then given by  $\langle r_{^9\text{Li}}^2 \rangle = \frac{4}{9}\langle r_{s_{1/2}}^2 \rangle + \frac{5}{9}\langle r_{p_{3/2}}^2 \rangle$ , where  $\langle r_{s_{1/2}}^2 \rangle$  and  $\langle r_{p_{3/2}}^2 \rangle$  are the mean square radii of the  $s_{1/2}$  and  $p_{3/2}$ -orbits, respectively.

If we use gaussian potentials for  $s$  and  $p$ -waves with equal range,  $V^{(\ell)} = S^{(\ell)} \exp(-r^2/b^2)$ , we can estimate the range of the interaction by using that i) the root mean square radius of  $^9\text{Li}$  is 2.32 fm, ii) the lowest  $s$ -state must be bound and the second must correspond to a low lying neutron virtual state in  $^{10}\text{Li}$ , and iii) the  $p$ -potential must have a bound state with a neutron separation energy around 4.1 MeV [16,17]. The precise position of the  $p_{3/2}$ -state is not important in the present work and we shall use the value 4.1 MeV obtained for  $^9\text{Li}$  even though the potential applies to the neutron- $^9\text{Li}$  system. The  $s_{1/2}$  and  $p_{3/2}$  bound states in this potential then produce a  $^9\text{Li}$  density distribution which strictly speaking is that of the core particles in  $^{10}\text{Li}$ . This is lack of selfconsistency in line with an inert core approximation, but only applied to estimate the range of the potential. This is only of marginal importance provided the resonances and virtual states remain unchanged.

In table 1 we show these potentials fulfilling conditions ii) and iii) for three different ranges of the gaussian. In all the three cases the  $s$ -potentials have only a bound state and a virtual state around 300 keV, and the  $p$ -potential has only a bound state at -4.1 MeV. As we can see in the table, only a range of around 2.0 fm is giving rise to a root mean square radius for  $^9\text{Li}$  in agreement with the experimental value of 2.32 fm.

We then turn to the valence neutrons, where we take a neutron- $^9\text{Li}$  potential with central, spin-spin, and spin-orbit terms

$$V_{nc}^{(\ell)}(r) = V_c^{(\ell)}(r) + V_{ss}^{(\ell)}(r)\langle \mathbf{s}_n \cdot \mathbf{s}_c \rangle + V_{so}^{(\ell)}(r)\boldsymbol{\ell}_{nc} \cdot \mathbf{s}_n, \quad (8)$$

Table 1

Parameters of the trial potentials  $V^{(\ell=0,1)} = S^{(\ell=0,1)} \exp(-r^2/b^2)$  used for the occupied  $s_{1/2}$  and  $p_{3/2}$ -levels in  ${}^9\text{Li}$ . The  $s$ -potential has a single bound state and a virtual state around 300 keV. The  $p$ -potential has a single bound state at  $-4.1$  MeV. The root mean square radius  $\langle r_{9\text{Li}}^2 \rangle^{1/2}$  of  ${}^9\text{Li}$  is obtained from the mean square radii  $\langle r_{s_{1/2}}^2 \rangle$  and  $\langle r_{p_{3/2}}^2 \rangle$  of the  $s$  and  $p$ -orbits, respectively.

	b=1.5 fm	b=2.0 fm	b=2.5 fm
$S^{(\ell=0)}$ (MeV)	-172.0	-95	-60
$\langle r_{s_{1/2}}^2 \rangle^{1/2}$ (fm)	1.27	1.51	1.90
$S^{(\ell=1)}$ (MeV)	-142.2	-86.2	-59.7
$\langle r_{p_{3/2}}^2 \rangle^{1/2}$ (fm)	2.36	2.79	3.18
$\langle r_{9\text{Li}}^2 \rangle^{1/2}$ (fm)	1.95	2.31	2.69

where  $\langle \mathbf{s}_n \cdot \mathbf{s}_c \rangle = \langle \ell_{nc}, j_n, J | \mathbf{s}_n \cdot \mathbf{s}_c | \ell_{nc}, j_n, J \rangle$ ,  $\mathbf{s}_n$  and  $\mathbf{s}_c$  are the intrinsic spins of the neutron and the core,  $\ell_{nc}$  is their relative orbital angular momentum,  $j_n$  is the coupled momentum of  $\ell_{nc}$  and  $s_n$ , and  $J$  is the total angular momentum obtained after coupling of  $j_n$  and the spin of the core  $s_c$ . Each level of the  ${}^{10}\text{Li}$  spectrum is specified by the quantum numbers  $\{\ell_{nc}, j_n, J\}$ . In particular, for  $s_{1/2}$ -waves ( $\ell_{nc}=0$ ,  $j_n=1/2$ ) the total angular momentum  $J$  can be either 1 or 2. Since the  ${}^9\text{Li}$ -core has negative parity the two possible  $s_{1/2}$ -virtual states are  $J^\pi = 1^-$  and  $J^\pi = 2^-$ -states. In the same way there are two possible  $p_{1/2}$ -resonances ( $\ell_{nc}=1$ ,  $j_n=1/2$ ) with  $J^\pi = 1^+$  and  $J^\pi = 2^+$ . We will refer equally to the two  $s_{1/2}$ -virtual states or the doublet  $1^-/2^-$  and to the  $p_{1/2}$ -resonances or the doublet  $1^+/2^+$ .

The radial shapes of the potentials in eq.(8) are chosen as gaussians with strengths adjusted independently for each value of  $\ell_{nc}$ . Since the range of the gaussians all are equal ( $b = 2.0$  fm), only the strengths remain as adjustable parameters depending on orbital angular momentum. In table 2 we show, as function of strengths, the position of the virtual states for  $\ell_{nc} = 0$  and the resonance energies and widths for  $\ell_{nc} = 1$ . Both virtual states and resonances are obtained as poles of the  $S$ -matrix. In previous works we often approximated by using the scattering length for  $s$ -waves and values where the phase shift equals  $\pi/2$  for  $p$ -resonances [30]. These energies are systematically slightly higher than the ones obtained from the  $S$ -matrix.

Summarizing, the neutron- ${}^9\text{Li}$  interaction is given by eq.(8), where the three strengths of the three gaussian potentials are parameters. For  $s$ -wave the spin-orbit part does not contribute and only two parameters remain, the central and the spin-spin potential. The first determines the average energy of the  $1^-$  and  $2^-$  levels, and the second one is separating these two states. For the  $p$ -waves we start by including only the central and spin-orbit terms in eq.(8). One of

Table 2

Strengths ( $S$ ) for the  $s$  and  $p$  neutron- ${}^9\text{Li}$  gaussian interactions. The energies of the corresponding virtual  $s$ -states are  $E_s$ , and energies and widths of the  $p$ -resonances are  $E_p$  and  $\Gamma$ . These parameters are precisely defined by real and imaginary values of the poles of the  $S$ -matrix.

$\ell_{nc} = 0$		$\ell_{nc} = 1$		
$S$ (MeV)	$E_s$ (keV)	$S$ (MeV)	$E_p$ (MeV)	$\Gamma$ (MeV)
-99.0	65	-68.0	0.23	0.09
-98.0	110	-67.5	0.30	0.14
-97.0	168	-67.0	0.37	0.18
-96.0	240	-66.5	0.44	0.24
-95.0	326	-66.0	0.50	0.30
-94.0	428	-65.5	0.57	0.38
-93.0	546	-65.0	0.63	0.44
-92.0	682	-64.5	0.69	0.52
-91.0	837	-64.0	0.76	0.59

these two strengths is determined such that the neutron  $p_{3/2}$ -state remains at -4.1 MeV corresponding to a strength  $V_c^{(\ell=1)} + 0.5V_{so}^{(\ell=1)} = -86.2$  MeV, as given in table 1. The  $p_{1/2}$ -strength parameter  $V_c^{(\ell=1)} - V_{so}^{(\ell=1)}$  can then be used to vary the resonance energy. On top of these ordinary central plus spin-orbit neutron-core terms, the potential in eq.(8) contains the spin-spin neutron-core interaction (spin-splitting term) which separates the  $1^+$  and  $2^+$ -states and the  $1^-$  and  $2^-$ -states.

A very important characteristic of this potential is that the  $s_{1/2}$ -interaction (typical strengths are given in table 2) has a low-lying virtual state and a deeply bound state while the  $p_{3/2}$ -interaction has a bound state at -4.1 MeV. Since the  $s_{1/2}$ -shell and the neutron  $p_{3/2}$ -shell are completely filled by the neutrons in the  ${}^9\text{Li}$  nucleus these states are forbidden by the Pauli principle when adding more neutrons as for  ${}^{10}\text{Li}$  and  ${}^{11}\text{Li}$ .

We avoid these orbits by use of the phase equivalent potentials [37,38] for the  $s_{1/2}$  and  $p_{3/2}$ -interactions. These potentials have exactly the same phase shifts as the initial ones, but the bound states are not present. They decrease exponentially at large distances and diverge as  $1/r^2$  at short distances. In other words, for the  $s_{1/2}$ -interaction we take potentials as in table 2, and for the  $p_{3/2}$ -interaction we use the one specified in the third column of table 1 for  $p$ -waves. For use in the three-body calculation we subsequently, as in [39], construct their respective phase equivalent potentials, which finally are used in eq.(2).

We have used  $l$ -dependent potential already by adjusting the strengths in eq.(8) independently for each partial wave. It certainly would have been possible to use  $l$ -independent potentials with complicated radial form factors and still reproduce the same properties. However, the phase equivalent potentials used to account for the Pauli principle also introduce  $l$ -dependent potentials. The simplicity of single gaussian form factors is then preferred since the potentials in the three-body computation in any case would be  $l$ -dependent.

It is well established that use of two-body interactions reproducing low-energy scattering properties leads to a three-body system that is marginally underbound compared to experimental values [40]. To fine tune the crucial three-body energy we include a three-body interaction,  $V_3(\rho)$ , in eq.(3). This is a phenomenological way of accounting for those polarizations of the particles that are beyond that described by the two-body interactions [41]. This is off-shell behavior possibly revealed in the three-body system. Thus, this interaction must be of short range, since it only contributes when all three particles interact simultaneously.

We also use a gaussian shape for this three-body potential. Since the hyperradius  $\rho$  corresponding to  ${}^9\text{Li}$  and two neutrons touching each other is approximately equal to 3.0 fm we use this value as the range for this three-body force. Nevertheless the precise value of the range is not essential and ranges between 2.5 and 4.0 fm all lead to very similar results. Another form factor of longer range for example exponential or falling off with a power law dependence of the hyperradius would increase the total radius. We maintain the gaussian shape and leave the strength of the three-body force as a parameter adjusted to recover the experimental  ${}^{11}\text{Li}$  binding energy of  $295 \pm 35$  keV [32]. In the calculations we shall use 0.30 MeV when adjusting to the measured binding energy.

## 4 Properties of ${}^{11}\text{Li}$

Experimental data and previous theoretical investigations established that  ${}^{10}\text{Li}$  has a low-lying virtual  $s$ -state close to 50 keV and a  $p_{1/2}$ -resonance at around 0.50 MeV. Furthermore, a neutron-core  $p$ -wave content in the  ${}^{11}\text{Li}$  wave function of around 40% is necessary to describe the momentum distributions obtained after fragmentation of  ${}^{11}\text{Li}$ . The unknowns in the present context are then essentially the energies of the second  $s_{1/2}$ -virtual state and the second  $p_{1/2}$ -resonance. We adjust the three-body potential to reproduce the crucial binding energy of about 0.30 MeV. In this section we investigate which sets of these  ${}^{10}\text{Li}$  energies are consistent with the established properties of  ${}^{11}\text{Li}$ .

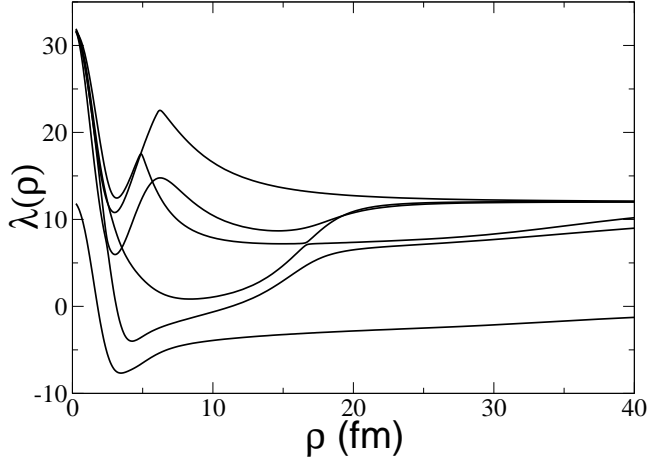


Fig. 1. The  $\lambda$ -spectrum as function of  $\rho$  for  $^{11}\text{Li}$  corresponding to average energies in  $^{10}\text{Li}$  for the virtual  $s$ -states and  $p_{1/2}$ -resonances of around 0.4 MeV. The  $s_{1/2}$  and the  $p_{3/2}$ -potentials are constructed as phase equivalent to deep potentials but now without any bound states.

#### 4.1 Effective radial potentials

Let us begin by computing the  $^{11}\text{Li}$  wave function without including the spin-spin term in eq.(8). This means that the  $1^-/2^-$  and the  $1^+/2^+$  doublets are degenerate. The energy of these two doublets corresponds then to the average energy of the doublet after a subsequent inclusion of the spin-spin potential. In [27] we have shown that the main properties of  $^{11}\text{Li}$  as well as the behavior of the momentum distributions are determined basically by these average energies. The most sensitive observable to the precise positions of the two  $s_{1/2}$ -virtual states and the two  $p_{1/2}$ -resonances is the invariant mass spectrum.

Without inclusion of the spin-spin term the  $s_{1/2}$ -interaction has only one free parameter, the strength of the gaussian, used to place the low-lying virtual  $s$ -state at the desired value. Since the  $p_{3/2}$  strength of  $-86.2$  MeV is fixed, the  $p$ -potential with both central and spin-orbit terms has also only one free parameter which controls the average energy of the  $p_{1/2}$ -resonances.

The first step is to compute the angular eigenvalue spectrum by solving the Faddeev equations in eq.(2). We show a typical example in fig. 1 for  $^{11}\text{Li}$  where all  $s$  and  $p$ -wave components are included and in addition also all  $d$ -waves with total  $L=0$  or 1. The average energies of the  $1^-/2^-$  and the  $1^+/2^+$  doublets are placed at around 0.4 MeV corresponding to strengths of  $-94.0$  MeV and  $-67.0$  MeV for the  $s_{1/2}$  and the  $p_{1/2}$ -potentials, respectively, see table 2. These eigenvalues define the effective radial potentials, which through eq.(3) lead to the radial wave function and the three-body energy. Although six eigenvalues are shown in fig. 1, only the three lowest are needed to get an accurate  $^{11}\text{Li}$  wave function and the two lowest already account for more than 98% of the

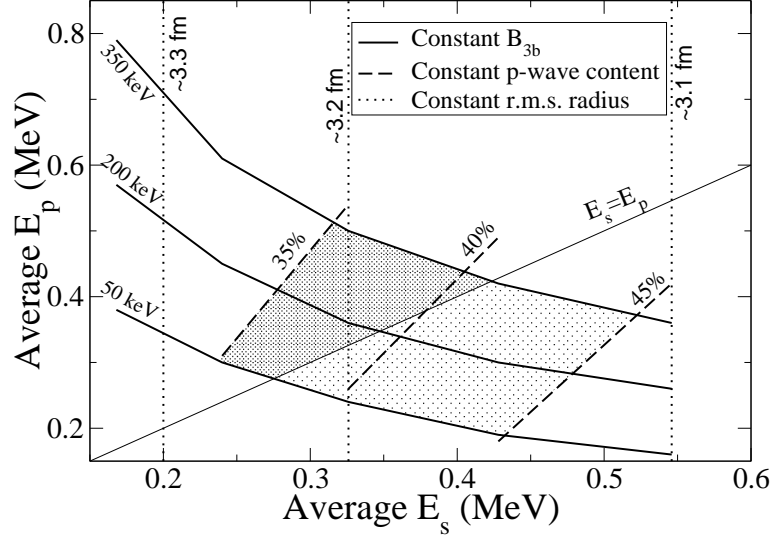


Fig. 2. Properties of the  $^{11}\text{Li}$  wave function as function of the statistically weighted average energies of the two virtual  $s_{1/2}$ -states ( $E_s$ ) and the two  $p_{1/2}$ -resonances ( $E_p$ ). The total three-body binding energy is 0.30 MeV consistent with the measurement. Along the solid lines we have constant binding energy contributions  $B_{3b} \equiv -\langle V_3(\rho) \rangle$  of the expectation value of the three-body force for the corresponding solutions. Along the dashed lines the  $p$ -wave content in the  $^{11}\text{Li}$  wave function is constant and along the dotted lines the root mean square radius is constant. The thin solid line indicates when the average  $s_{1/2}$  and  $p_{1/2}$ -energies are equal. The shaded regions between the lines labeled 35%, 45%, 50 keV and 350 keV, indicate the possible values for the average  $s_{1/2}$  and  $p_{1/2}$ -energies.

total norm. This is intuitively clear from the attractive pockets around  $\rho \approx 4$  fm only appearing for the two lowest eigenvalues in fig. 1. We also see that the lowest  $\lambda$  is flat, with an attraction extending to relatively large distances. This is a combined effect of the large neutron-neutron and neutron- $^9\text{Li}$   $s$ -wave scattering lengths [42].

The  $\lambda$ -spectrum at the origin and at infinity usually corresponds to the hyperspherical spectrum  $K(K+4)$ , where  $K$  is the hypermomentum [2,25]. A calculation for  $^{11}\text{Li}$  as described above, but with two-body potentials without bound states leads to a spectrum with one  $\lambda$  starting from 0 ( $K=0$ ) and five  $\lambda$ 's from 12 ( $K=2$ ). However, the existence of Pauli forbidden  $s_{1/2}$  and  $p_{3/2}$ -states and the use of phase equivalent potentials to exclude them from the three-body calculation is modifying the  $\lambda$ -spectrum at short distances [39]. In fact, as seen in fig. 1, the  $\lambda$  starting at 0, and four of the  $\lambda$ 's starting at 12 have disappeared, but the original spectrum (one  $\lambda$  at 0 and five at 12) is preserved at large distances.

## 4.2 Variation with spin averaged parameters

The statistically weighted average values of the two  $s_{1/2}$ -energies and correspondingly of the two  $p_{1/2}$ -energies are the crucial quantities. The individual positions are only important for very specific observables. In the following we shall refer to these combinations simply as average values. The two free parameters are now used to vary these average energies of the (unbound)  $s_{1/2}$  and  $p_{1/2}$ -states in  $^{10}\text{Li}$ . The resulting properties of the  $^{11}\text{Li}$  wave function are shown in fig. 2. Selecting a set of these two parameters does not automatically produce a bound  $^{11}\text{Li}$  system. In any case the expectation value  $-B_{3b} \equiv \langle V_3(\rho) \rangle$  of the three-body potential, where the wave function used in the expectation value is that of the three-body solution, must vary with the parameters. The total energy is decisive for many properties and we therefore adjust the three-body force,  $V_3(\rho)$ , in eq.(2) to give a total three-body binding energy of 0.30 MeV for  $^{11}\text{Li}$ . Then the strength of the gaussian  $V_3(\rho)$  potential is a function of the  $^{10}\text{Li}$  parameters. We show the curves of constant three-body binding energy corresponding to  $B_{3b}$  50 keV, 200 keV and 350 keV. Almost independent of  $E_p$  we obtain the curves of constant radii, i.e. 3.1 fm, 3.2 fm and 3.3 fm. The lines of constant  $p$ -wave content, 35%, 40%, and 45%, must correspond to simultaneous increase of the weighted average values of both  $s$  and  $p$ -energies. From fig. 2 we can already extract relevant information:

- Values of the average  $p_{1/2}$ -energy, giving rise to a  $^{11}\text{Li}$  structure with a  $p$ -wave content around 40% compatible with the known fragmentation data, are always below 0.5 MeV. Energies above this value require a large energy contribution from the three-body force, and also a rather high value of the average  $s_{1/2}$ -energy. Therefore the lowest  $p_{1/2}$ -state in  $^{10}\text{Li}$  can not be above 0.5–0.6 MeV.
- In the same way, reasonable values of the average  $p_{1/2}$ -energy are always above 0.2 MeV. Lower values would lead to a too bound  $^{11}\text{Li}$  wave function, or at least with a very little effect of the three-body force. The possibility of very high values of the  $s_{1/2}$ -energy leads to a too small r.m.s. radius substantially below 3.1 fm and would in addition require essentially zero spin-splitting to avoid binding of  $^{10}\text{Li}$ . Therefore 0.2 MeV is the lowest limit for the average  $p_{1/2}$ -energy, implying that the highest  $p_{1/2}$ -resonance has to be above this value.
- The values of the average  $s_{1/2}$ -energy, giving a  $^{11}\text{Li}$  with reasonable size, binding and  $p$ -wave content, range between 250 keV and 550 keV.
- An average  $s_{1/2}$ -energy below the average  $p_{1/2}$ -energy requires  $p$ -wave contents between 35% and 40%. Higher  $p$ -wave contents need the  $s_{1/2}$ -energy above the  $p_{1/2}$ -energy.
- A  $p$ -wave content around 50%, as suggested in [20], needs an average  $p_{1/2}$ -energy below 0.3–0.4 MeV, and a significantly higher average  $s_{1/2}$ -energy close to 600 keV. In any case the size of such  $^{11}\text{Li}$  would be clearly smaller

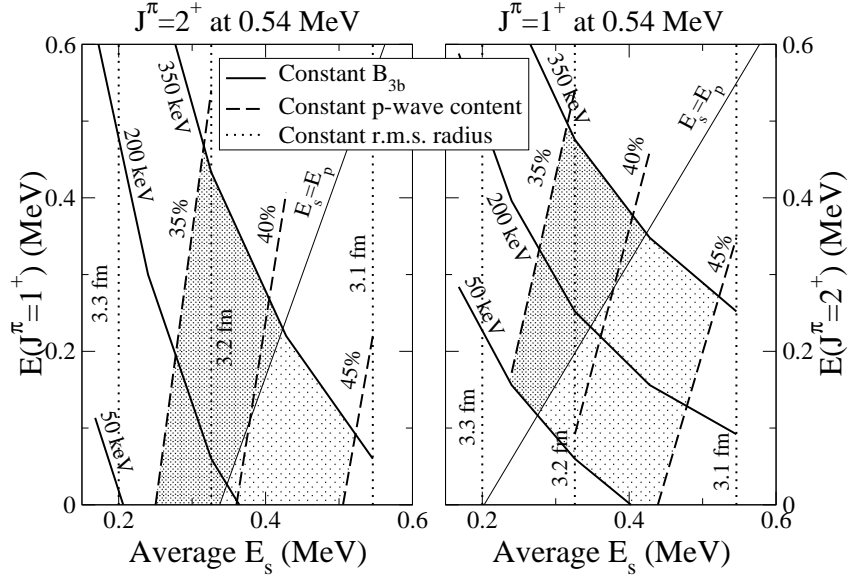


Fig. 3. Left: Properties of the  $^{11}\text{Li}$  wave function as function of the average energy of the two virtual  $s$ -states ( $E_s$ ) and the energy of the  $1^+$   $p$ -resonance when the  $2^+$   $p$ -resonance is kept at 0.54 MeV. Right: The same as the left part but now as function of the energy of the  $2^+$   $p$ -resonance with the  $1^+$   $p$ -resonance fixed at 0.54 MeV. The meaning of the curves is as in fig. 2.

than 3.1 fm, the lower limit of the radius.

- A r.m.s. larger than 3.3 fm produces a  $^{11}\text{Li}$  with too little  $p$ -wave content, not higher than 25%.
- Therefore, the regions of possible values for the average  $s_{1/2}$  and  $p_{1/2}$ -energies are the shaded regions in fig. 2, where we assumed that  $^{11}\text{Li}$  has a  $p$ -wave content between 35% and 45%, that the limits of the r.m.s. radius of  $^{11}\text{Li}$  are  $3.2 \pm 0.1$  fm and finally that the three-body computations need a finite three-body force. The dark shade corresponds to average  $s$ -energies below the  $p_{1/2}$ -energies, while the lighter area is the other way around. There is no requirement of an average  $s_{1/2}$ -energy below that of  $p_{1/2}$ . A sufficiently large spin-splitting in the  $s_{1/2}$ -interaction could produce the experimentally required very low-lying  $s_{1/2}$ -virtual state and simultaneously maintain the average  $s$ -energy above the average  $p_{1/2}$ -energy.
- One of the most firmly established properties of the  $^{10}\text{Li}$  spectrum is the existence of a  $p_{1/2}$ -resonance at around 0.5 MeV. According to fig. 2 another  $p_{1/2}$ -resonance must be present at an energy below 0.5 MeV in order to maintain the average energy in the shaded region. The only experimental evidence for this low-lying  $p$ -resonance is the Berlin group [12] giving an energy of  $0.24 \pm 0.06$  MeV.



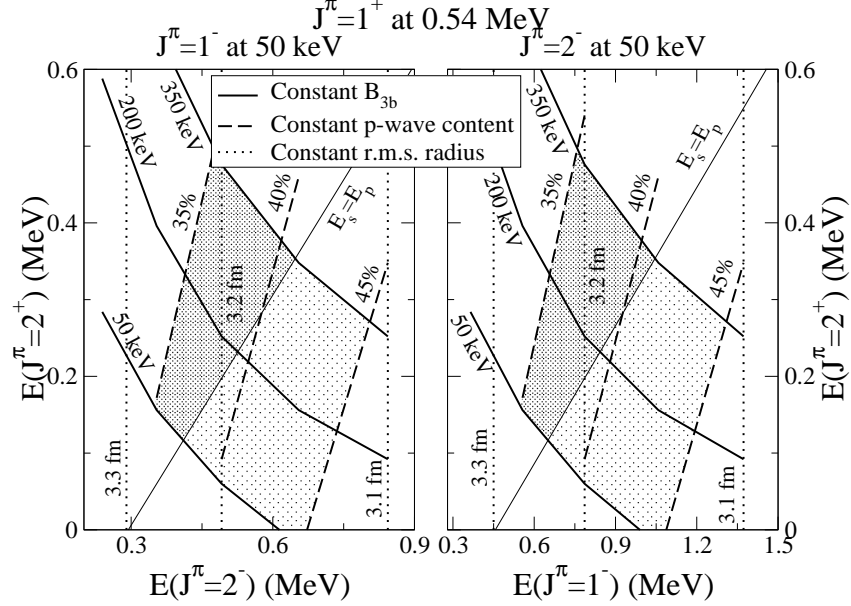


Fig. 4. Left: Properties of the  $^{11}\text{Li}$  wave function as function of the energies of the  $2^-$  and the  $2^+$ -energies when the  $1^+$ -resonance is at 0.54 MeV and the  $1^-$  is at 50 keV. Right: The same as the left part but now as as function of the  $1^-$  energy with a fixed  $2^-$ -state at 50 keV.

#### 4.3 Effects of spin splitting

Let us now in the potential (8) consider the spin-spin term which also is assumed to be a gaussian with the same range ( $b = 2.0$  fm) as the central and spin-orbit terms. Inclusion of this term in the  $p$ -potential separates the two  $p_{1/2}$ -resonances and the strength of the gaussian can then be used to split the energy of these resonances. We show in fig. 3 the same kind of plot as in fig. 2, but now with a fixed energy of 0.54 MeV for one of the  $p_{1/2}$ -resonances. Thus we show the properties of  $^{11}\text{Li}$  as function of the average  $s_{1/2}$ -energy and the  $2^+$  (left part) or  $1^+$  (right part)  $p$ -resonances fixed at 0.54 MeV. Again the shaded areas correspond to the region consistent with the established properties of  $^{11}\text{Li}$ .

In both parts of the figure we confirm clearly that a  $p_{1/2}$ -resonance at 0.54 MeV necessarily needs a second  $p_{1/2}$ -resonance at a lower energy. If the resonance,  $J^\pi = 2^+$ , is at 0.54 MeV (left part) then the  $J^\pi = 1^+$  resonance can occur at very low values. In fact, if we consider  $^{11}\text{Li}$  with 40%  $p$ -wave content and a binding energy contribution of the three-body force of 200 keV then the  $1^+$ -resonance would be very close to threshold. A  $1^+$ -state at 0.24 MeV (as suggested in [12]) would require either a  $p$ -wave content smaller than 40% or a large contribution to the energy of the three-body force. The maximum value for the  $1^+$ -resonance is around 0.4 MeV.

If the  $J^\pi = 1^+$  resonance is at 0.54 MeV (right part) then the  $2^+$ -state can

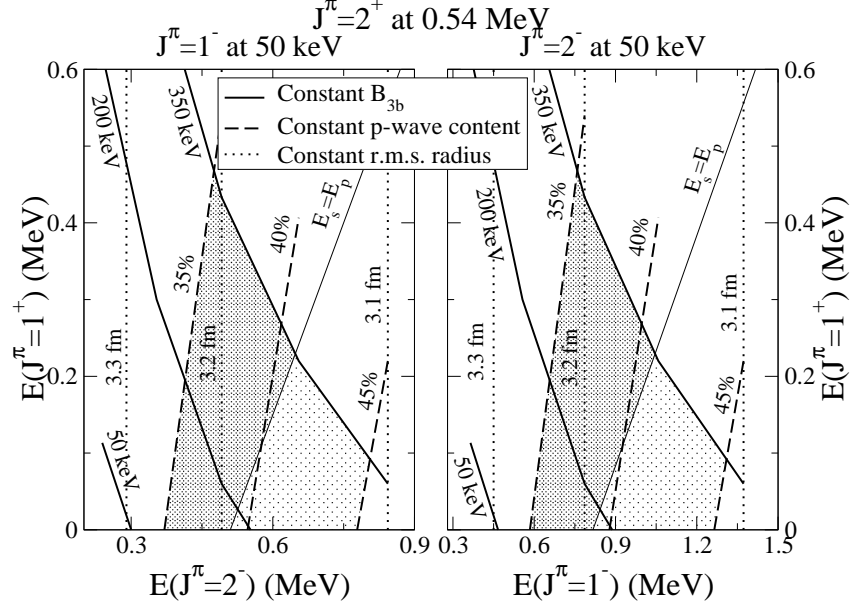


Fig. 5. The same as fig. 4 but fixing the  $2^+$  energy at 0.54 MeV and plotting the  $^{11}\text{Li}$  properties as function of the  $1^+$  energy.

also occur at low values, although in this case resonances close to threshold have a  $p$ -wave content close to 45% and a smaller contribution to the energy from the three-body force. Then a  $^{11}\text{Li}$  structure with around 40%  $p$ -wave and binding energy contribution of the three-body force close to 200 keV is consistent with a second  $p_{1/2}$ -resonance at  $0.24 \pm 0.06$  MeV. The maximum values for the  $2^+$  are still around 0.4 MeV.

In figs. 2 and 3 we considered average energies for the  $s_{1/2}$ -states and we concluded that values between 250 and 550 keV are in agreement with the known properties of  $^{11}\text{Li}$ . Experimentally the existence of a very low-lying  $s$ -state close to 50 keV is known. We then use the spin-splitting term of the potential for  $s$ -waves to fix one of the two  $s_{1/2}$ -virtual states at 50 keV. In fig. 4 we fix the  $1^+$ -resonance at 0.54 MeV (as in the right part of fig. 3) and fix one of the  $s_{1/2}$ -states at 50 keV (the  $1^-$  in the left part and the  $2^-$  in the right part). We then plot the properties of  $^{11}\text{Li}$  as function of the  $2^+$  and  $2^-$  energies in the left part of the figure and as function of the  $2^+$  and  $1^-$  energies in the right part of the figure.

We see that inclusion of the spin-splitting potential for  $s$ -waves does not change the conclusions about the  $2^+$  energy compared to the left part of fig. 3, and the only new information is that if the  $2^-$  state is at 50 keV, then the  $1^-$ -energy moves between 0.6 and 1.2 MeV. On the other hand, if the virtual state at 50 keV is the  $1^-$ -state then the second  $s$ -state is at an energy between 400 and 750 keV. The same is observed in fig. 5, constructed in analogy to fig. 4, but with the  $2^+$ -resonance at 0.54 MeV. Then fig. 5 corresponds to the left part of fig. 3 after including the spin-splitting term in the  $s$ -potential.

#### 4.4 The $^{10}\text{Li}$ spectrum

The information obtained from figs. 4 and 5 can now be used to predict the spectrum of  $^{10}\text{Li}$  for different properties of  $^{11}\text{Li}$  while assuming a  $p_{1/2}$ -resonance at 0.54 MeV and a low-lying  $s_{1/2}$ -state at 50 keV. For instance, if we assume a  $p$ -wave content of 40% and a 350 keV for  $B_{3b}$  the energies of the remaining two  $^{10}\text{Li}$  states are determined where these curves cross each other. From the left part of fig. 4 we find an energy for the  $2^+$  state close to 0.4 MeV, and a bit above 0.6 MeV for the  $2^-$ -state. The resulting spectrum of  $^{10}\text{Li}$  for this case is shown in column (a) of the upper part of fig. 6. From the right part of fig. 4 we find that the  $2^-$ -state is at 50 keV and the  $1^-$ -state is then close to 1 MeV. This spectrum is shown in column (b) of the upper part of fig. 6.

In the same way, assuming a  $p$ -wave content of 40% and  $B_{3b} = 350$  keV, we obtain from the left and right part of fig. 5 the spectra shown in columns (c) and (d) of fig. 6. We observe that these two cases are consistent with the  $1^+$ -level at  $0.24 \pm 0.06$  MeV and the  $2^+$ -level at  $0.54 \pm 0.06$  MeV observed in [12]. The average energy for the  $s_{1/2}$ -levels is close to 0.4 MeV in all the four cases, and it is a bit below the value around 0.45 MeV of the  $p_{1/2}$ -levels.

Although a  $p$ -wave content of 40% is consistent with previous calculations, the energy given by the three-body force is not known. In the central part of fig. 6 we show the same spectra for  $^{10}\text{Li}$  as in the upper part but assuming  $B_{3b} = 200$  keV. The four spectra correspond to the crossing between the  $B_{3b} = 200$  keV line and the line showing a  $p$ -wave content of 40% in the left and right parts of figs. 4 and 5, respectively. Now the average energy of the  $p$ -resonances is slightly lower than the energy of the  $s$ -states and both of them are smaller than those from the upper part. This is because the two-body interactions give more binding than in the previous case.

Columns (a) and (b) of these spectra can also be consistent with a second  $p_{1/2}$ -resonance around 0.24 MeV, although now this resonance corresponds to the  $2^+$ -level instead of the  $1^+$ -level as given in [12]. In the spectra (c) and (d) in the central part of fig. 6 the lowest  $p_{1/2}$ -resonance is very close to threshold (the crossing between  $B_{3b} = 200$  keV and  $p$ -wave content of 40% in fig. 5 is very close to zero  $1^+$ -energy). As previously indicated there is no experimental evidence of such a low  $p_{1/2}$ -resonance, and it is established that the ground state corresponds to an  $s_{1/2}$ -state.

Finally, in the lower part of fig. 6 we show the  $^{10}\text{Li}$  spectrum by assuming  $B_{3b} = 50$  keV. Again, since the three-body force is providing less binding the average energy of the  $s$ -states and the  $p$ -resonances is smaller than in the previous cases. The role played by the three-body force is now not very important.

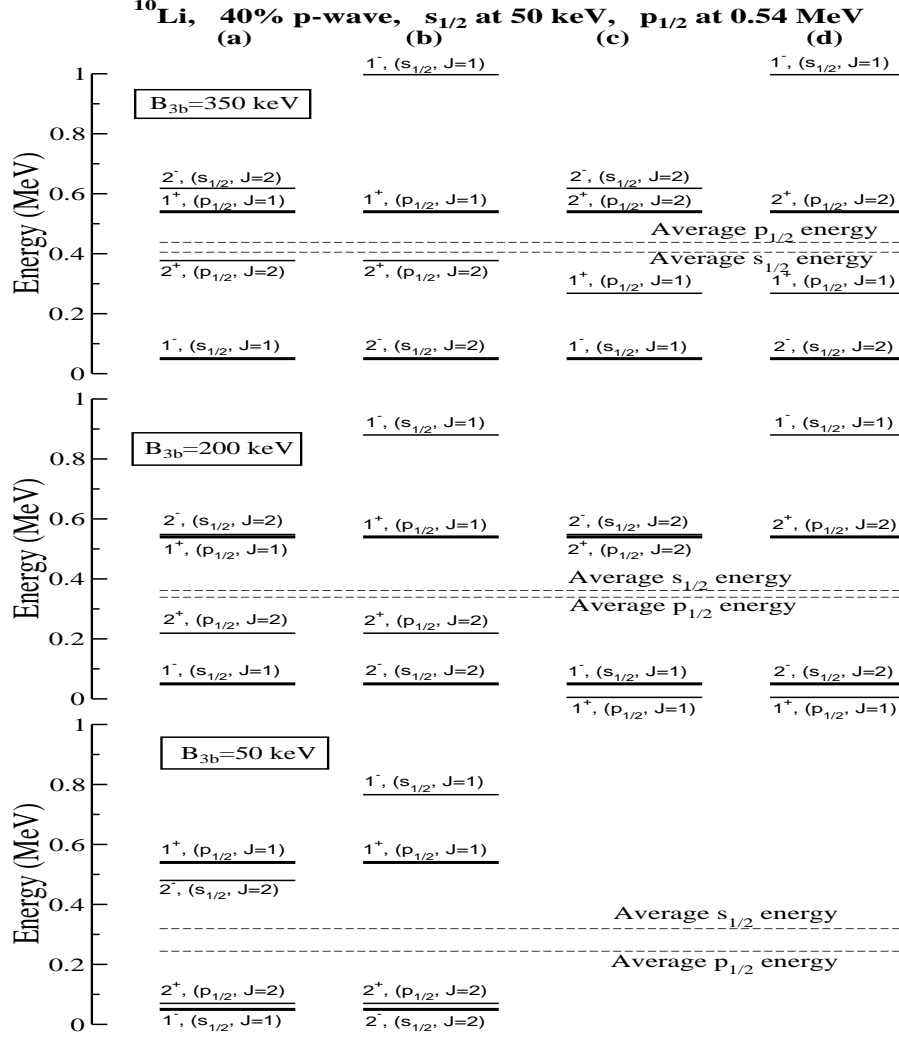


Fig. 6. Spectra for  $^{10}\text{Li}$  assuming an  $s_{1/2}$ -virtual state at 50 keV, a  $p_{1/2}$ -resonance at 0.54 MeV, and a  $p$ -wave content of 40%. The upper, central, and lower parts show the cases where  $B_{3b} = 350$  keV, 200 keV, and 50 keV, respectively. Columns (a), (b), (c), and (d) correspond to the cases shown in the left part of fig. 4, right part of fig. 4, left part of fig. 5, and right part of fig. 5, respectively. Levels indicated with a thick line are the  $s$  and  $p$ -levels for which the energy have been fixed at 50 keV and 0.54 MeV, respectively.

The crossing between the lines corresponding to constant  $B_{3b}=50$  keV and constant  $p$ -wave content of 40% in fig. 4 gives rise to the two spectra shown in the figure. In this case also a  $p_{1/2}$ -resonance (the  $2^+$ -state) appears at an energy below 100 keV.

From fig. 5 the same procedure gives negative energies of the  $1^+$ -level, meaning that this level is bound. This is of course against the well known fact that  $^{10}\text{Li}$  is not bound, and the corresponding  $^{10}\text{Li}$  spectrum can certainly not correspond to the real one. Actually, from the spectra (c) and (d) in the middle part of

Table 3

Strength parameters in MeV of the two-body neutron- $^9\text{Li}$  potentials of the form  $V_i^{(\ell)} = S_i^{(\ell)} \exp(-r^2/b^2)$ , where  $i = c, ss, so$ , see eq.(8). The strengths of the three-body potential of the form  $V_{3b} = S_{3b} \exp(-r^2/b_3^2)$  are given in MeV. The first column gives the sequence of quantum numbers of the spectrum in fig. 6 with the lowest first. The ranges are  $b = 2.0$  fm and  $b_3 = 3.0$  fm in all cases. The 10 different sets correspond to the spectra of fig. 6, where we start in the upper left corner taking line by line.

case	$S_c^{(\ell=0)}$	$S_{ss}^{(\ell=0)}$	$S_c^{(\ell=1)}$	$S_{so}^{(\ell=1)}$	$S_{ss}^{(\ell=1)}$	$S_{3b}$
1 $^-$ 2 $^+$ 1 $^+$ 2 $^-$	-94.0	6.85	-79.64	-13.12	-0.65	-3.9
2 $^-$ 2 $^+$ 1 $^+$ 1 $^-$	-94.0	-11.4	-79.64	-13.12	-0.65	-3.9
1 $^-$ 1 $^+$ 2 $^+$ 2 $^-$	-94.0	6.85	-79.64	-13.12	1.10	-3.9
2 $^-$ 1 $^+$ 2 $^+$ 1 $^-$	-94.0	-11.4	-79.64	-13.12	1.10	-3.9
1 $^-$ 2 $^+$ 1 $^+$ 2 $^-$	-94.6	6.10	-79.86	-12.68	-1.20	-2.3
2 $^-$ 2 $^+$ 1 $^+$ 1 $^-$	-94.6	-10.1	-79.86	-12.68	-1.20	-2.3
1 $^+$ 1 $^-$ 2 $^+$ 2 $^-$	-94.6	6.10	-79.86	-12.68	1.95	-2.3
1 $^+$ 2 $^-$ 2 $^+$ 1 $^-$	-94.6	-10.1	-79.86	-12.68	1.95	-2.3
1 $^-$ 2 $^+$ 2 $^-$ 1 $^+$	-95.0	5.55	-80.08	-12.25	-1.70	-0.8
2 $^-$ 2 $^+$ 1 $^+$ 1 $^-$	-95.0	-9.3	-80.08	-12.25	-1.70	-0.8

fig. 6, we already see that a value of  $B_{3b}$  slightly below 200 keV is already binding the 1 $^+$ -level.

For completeness we give in table 3 the two and three-body potentials corresponding to all the spectra shown in fig. 6.

#### 4.5 Invariant mass spectra in fragmentation reaction

According to the experimental and theoretical information collected about  $^{10}\text{Li}$  and  $^{11}\text{Li}$  we can conclude that the spectra shown in the upper part of fig. 6, especially in (c) and (d), and spectra (a) and (b) shown in the middle part, are the main candidates for the  $^{10}\text{Li}$ -spectrum. From the different observables obtained experimentally after fragmentation of  $^{11}\text{Li}$  the invariant mass spectrum is the observable most sensitive to the energies of the different resonances and virtual states. Investigation of the invariant mass spectrum could then help to establish which spectrum is most probable for  $^{10}\text{Li}$ .

In fig. 7 we show the invariant mass spectrum for all the  $^{10}\text{Li}$  spectra shown in fig. 6. The observables after fragmentation of  $^{11}\text{Li}$  are computed following

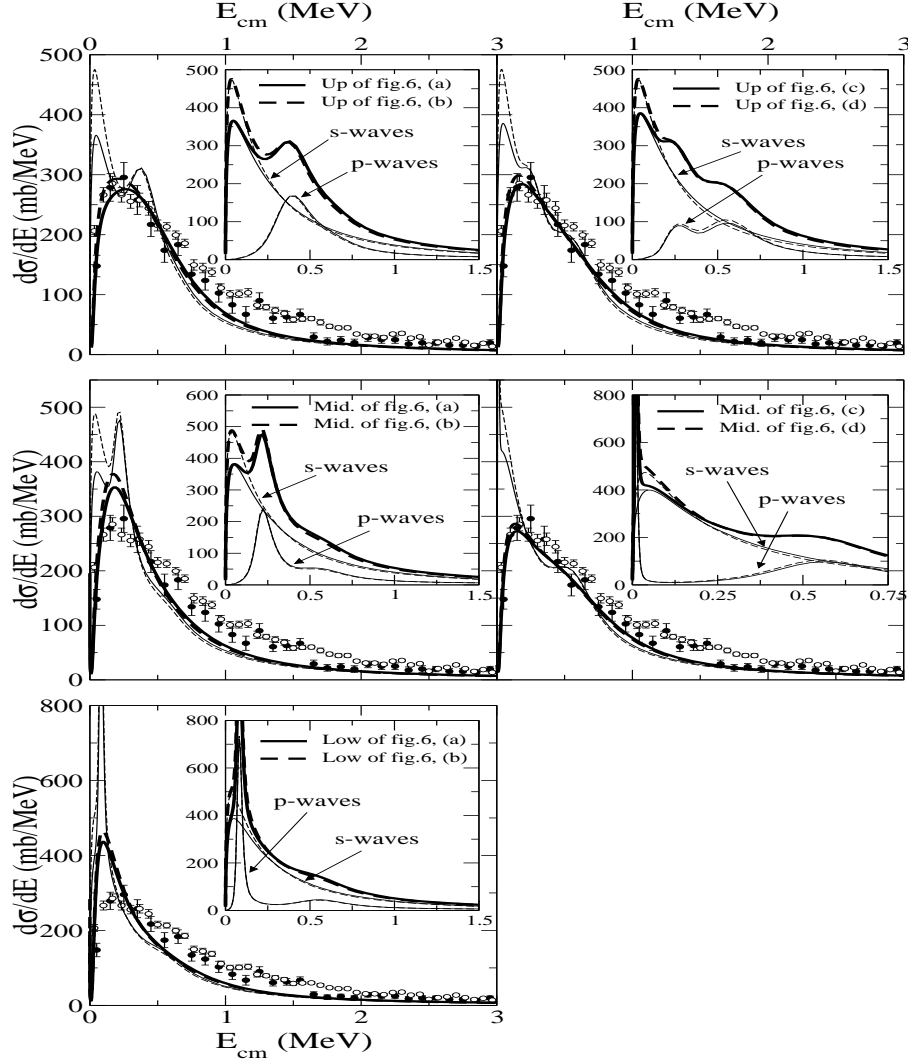


Fig. 7. Invariant mass distributions obtained with the different  $^{10}\text{Li}$  spectra shown in fig. 6. The upper, central, and lower parts correspond to the upper, central, and lower parts of fig. 6. Distributions in the left panels correspond to the  $^{10}\text{Li}$  spectra (a) solid lines, and (b) dashed lines of fig. 6, while the distributions in the right panels correspond to the  $^{10}\text{Li}$  spectra (c) solid lines, and (d) dashed lines of fig. 6. In the main plots we show the invariant mass distributions for each case and the results obtained after convoluting with the experimental beam profile. The internal plots show the invariant mass distributions and the contribution to the total from the  $s$ -waves and the  $p$ -waves. Experimental data are from [43] filled circles, and from [44] open circles.

the participant-spectator method described in [31]. The external parts of each graph in the figure show the computed invariant mass spectrum (thin lines) and the result after convoluting with the experimental beam profile (thick lines). This curve is compared with the experimental data taken from [43] and [44]. These sets of experimental data do not agree in the absolute numbers, and we have scaled those of [44] to the same maximum as in [43].

Note that the only difference between the  $^{10}\text{Li}$ -spectra (a) and (b) and between (c) and (d) is the ordering of the  $1^-$  and the  $2^-$ -levels. Therefore the compared solid lines and dashed lines in fig. 7 differ only in the ordering of the  $1^-/2^-$ -doublet. For the solid lines the  $1^-$ -state is at 50 keV, while for the dashed lines the  $2^-$ -state is at 50 keV.

As we can see in all the panels in fig. 7 the difference between solid and dashed lines is very small, especially after convoluting with the experimental beam profile. The only difference appears before convoluting and at very small energies, where the cases with the  $2^-$ -state at 50 keV (dashed lines) have a higher peak. This is due to the larger statistical weight of the  $2^-$ -level compared to the  $1^-$ -level (5/3 times bigger). In any case, from the invariant mass distributions and its comparison with the present experimental data it is not possible to determine which of the two states in the doublet  $1^-/2^-$  corresponds to the low-lying  $s$ -state found experimentally.

Let us concentrate now on the  $^{10}\text{Li}$ -spectra (a) and (b). In the three cases, upper, middle, and lower parts, one of the  $s$ -states is placed at 50 keV, and the  $1^+$ -resonance is fixed at 0.54 MeV. Basically the only difference between the three cases is the energy of the  $2^+$ -level, that goes from almost 0.4 MeV to a small value below 100 keV. Looking at the corresponding invariant mass distributions in the left part of fig. 7 we observe that calculations before convoluting with the experimental beam profile show two peaks corresponding to the low  $s$ -state at 50 keV, and the  $2^+$ -resonance. These two peaks approach each other when the energy of these two levels becomes closer, and the one corresponding to the  $2^+$ -resonance becomes higher when its energy approaches the threshold. In fact, in the lower part of fig. 7 both peaks can not be distinguished.

The peak corresponding to the  $1^+$ -state at 0.54 MeV can not be seen. Looking at the  $p$ -wave contribution (inner panels) we note that only in the lower part this peak can be noticed in the small bump produced in the total invariant mass distribution, although this bump disappears after convolution with the beam profile. The main effect produced by the different energies of the  $2^+$ -resonance is that the lower the energy of the state the narrower the computed invariant mass spectrum. This fact is preserved after convoluting the computed distributions with the experimental beam profile. The main effect of the convolution is that the separated peaks associated to the low-lying  $s$ -state and the  $2^+$ -resonance merge into one. In any case the comparison with the experimental distribution shows that the computed ones are too narrow, except perhaps for values of the  $2^+$ -level close or higher than 0.4 MeV. This would mean that the two states in the  $1^+/2^+$ -doublet would be almost degenerate. Therefore a  $2^+$ -level below the  $1^+$ -level is not likely.

Let us focus now on the  $^{10}\text{Li}$ -spectra (c) and (d). Again one of the  $s$ -levels is

placed at 50 keV, but now the  $2^+$ -level is fixed at 0.54 MeV, while the energy of the  $1^+$ -level takes different values. In the upper part the  $1^+$ -resonance has an energy of 0.25 MeV. The computed invariant mass spectrum shows two shoulders produced by the two  $p$ -resonances. These two states are clearly seen in the  $p$ -wave contribution shown in the inset of the upper part of fig. 7. Nevertheless the structure observed in the computed invariant mass spectrum disappears after convolution. The agreement with the experimental data is quite satisfactory, especially with the one given in [43]. If we reduce the energy of the  $1^+$ -level its contribution appears in a higher and narrower peak.

In the middle part of fig. 7 we show the extreme case in which the  $1^+$ -level is very close to the threshold (its energy is around 10 keV). As we see in the inset, the  $p$ -wave contribution has a wide peak at 0.5 MeV and a sharp and very high peak at a very low energy corresponding to the  $1^+$ -resonance. This is obviously producing a similar high and narrow peak in the computed invariant mass spectrum. Nevertheless after convolution this peak is not visible anymore, and the comparison with the experiment can also be considered rather good. This is because although convolution is diluting the presence of the sharp peak at low energies there is still a resonance at 0.54 MeV, with high statistical weight, that makes the tail of the total distribution behave accordingly. Therefore a  $1^+$ -level below the  $2^+$  is the most likely structure for the  $^{10}\text{Li}$ -spectrum. This result agrees with [12].

From the simultaneous analysis of figs. 6 and 7 we can then summarize the results in the following points: i) We can not establish which of the two states in the doublet  $1^-/2^-$  is the one at a very low energy, ii) a  $2^+$  resonance below the  $1^+$ -level is not likely, producing too narrow invariant mass spectra, unless the  $1^+$  and the  $2^+$ -states are close to degeneracy, iii) the most likely situation corresponds to a  $1^+$ -level below the  $2^+$ -state, although it can not be extracted by direct comparison with the experimental invariant mass spectra, (iv) experiments with a better beam energy resolution are desirable, since the predicted structure in the invariant mass spectra then could be detected and the results from the different spectra directly distinguished.

#### 4.6 Momentum distribution after fragmentation

As a final test, we show in fig. 8 some additional observables after fragmentation of  $^{11}\text{Li}$  on carbon. The calculations have been performed assuming the best candidates for the  $^{10}\text{Li}$  spectrum, i.e. the spectra (c) and (d) in the upper part of fig 6. The computed results for both spectra are completely indistinguishable. In part (a) of fig. 8 we show the core momentum distribution. The thin line is the pure calculation while the thick line is the result obtained after convoluting with the experimental beam profile [45]. In part (b) we show the



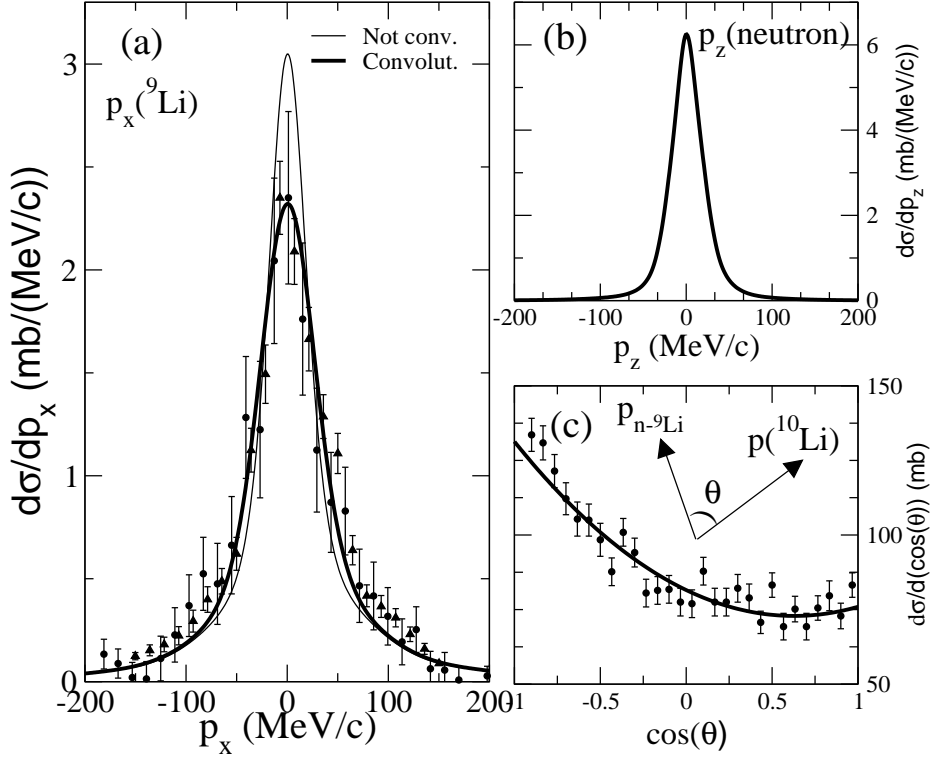


Fig. 8. (a) core momentum distribution, (b) parallel neutron momentum distribution, and (c) angular distribution after fragmentation of  ${}^{11}\text{Li}$  on carbon at 280 MeV/nucleon. In (a) the thin line is the computed curve and the thick line is the distribution obtained after convolution with the experimental beam profile. The experimental data are taken from [45,46] in (a) and from [29] in (c).

neutron momentum distribution, for which experimental data are not available yet. In part (c) we show the angular distribution, where  $\theta$  is the angle between the  ${}^{10}\text{Li}$  momentum and the relative momentum between neutron and core after the fragmentation. The curve is very sensitive to the  $s$  and  $p$ -wave mixing and the agreement is therefore a strong indication of a  $p$ -wave content of about 40%. For both the distributions in (a) and (c) the agreement with the experimental data is very good.

Finally we want to discuss the radius of  ${}^{11}\text{Li}$ . It has been extracted by model computations and fitting of measured interaction cross sections. The results depend somewhat on the assumed density distributions and the reaction models. We obtain interaction cross sections almost constant between 1030 and 1045 mb for a beam energy varying between 300 and 700 MeV/nucleon on a carbon target. This should be compared to the experimental values of  $1055 \pm 14$  mb at 800 MeV/nucleon and  $959 \pm 21$  mb at 400 MeV/nucleon. Also the measured interaction cross sections for heavier targets like copper and lead agree quite well with our model computations using the new neutron- ${}^9\text{Li}$  interaction. Our resulting root mean square radius is about 3.2 fm. It should perhaps be emphasized that a larger range and in particular another choice of

radial shape of the three-body interaction could be designed to increase the resulting radius by fractions of a fm possibly without changing anything else.

## 5 Summary and Conclusions

The recent measurements of the properties of  $^{10}\text{Li}$  confine the neutron- $^9\text{Li}$  interaction which is decisive for the elaborate three-body computations of  $^{11}\text{Li}$ . To use the new information the  $^{11}\text{Li}$  model must be realistic and in particular the hyperfine structure arising from spin-spin couplings must be included when the measured energy spectrum of  $^{10}\text{Li}$  is used for comparison.

We first sketch our method of adiabatic hyperspherical expansion of the Faddeev components to determine the structure of  $^{11}\text{Li}$  from a given set of two-body interactions. Second we sketch the participant-spectator reaction model used for all the fragmentation cross sections.

The neutron-neutron interaction is well known and not crucial as long as the scattering length and effective ranges are correct. The same could be said about the neutron- $^9\text{Li}$  interaction but in this case we do not have sufficient information. We believe that compelling experimental evidence show that an  $s$ -state is present at around 50 keV and a  $p$ -state around 0.5 MeV. We proceed by constructing an  $s$ -state neutron- $^9\text{Li}$  gaussian potential of range  $b$  with a deeply bound state and one very low-lying virtual state. We also construct a  $p_{3/2}$  gaussian potential with the same range  $b$  with a bound state at -4.1 MeV. These two potentials produce a density distribution of  $^9\text{Li}$  with the measured root mean square radius of 2.32 fm when  $b \approx 2$  fm. The core density and potential radius is now defined.

The three-body computation for  $^{11}\text{Li}$  with these interactions supplemented with an appropriate spin-orbit term would lead to a disaster since the additional two neutrons would occupy the low-lying Pauli forbidden states of the core-neutrons. Therefore we introduce the phase equivalent potentials for both  $s_{1/2}$  and  $p_{3/2}$  states. These potentials have precisely the same low-energy scattering properties but without the Pauli forbidden bound states. For weakly bound three-body systems this has proven to be an accurate procedure. Although technically difficult this is possible and above all this is a physically appropriate prescription to account for the most important many-body effect in the present context. The radial shapes of the potentials are not important provided the low-energy scattering properties are correct. Therefore we are content with using gaussians. The result is that we have two free strength parameters, one for  $s_{1/2}$  and one for  $p_{1/2}$ -states.

The last part of the neutron- $^9\text{Li}$  interaction arises from the  $^9\text{Li}$ -spin of 3/2

coupling to the neutron angular momenta of  $s_{1/2}$  and  $p_{1/2}$  resulting in two sets of spin-split states of opposite parity but the same spins of 1 and 2. Again we maintain the same range parameter  $b$  of a gaussian potential leaving us with two new strength parameters. These four parameters may be understood as related to the four different  $^{10}\text{Li}$ -states. In addition the properties of  $^{11}\text{Li}$  can now be used to constrain the parameters.

Unfortunately we must also use the three-body potential introduced to fine tune the three-body energy which is necessary even when using a set of two-body interactions reproducing all low-energy scattering properties. This must be a short range potential and we make it as neutral as possible under that assumption, i.e. we only use it to adjust the binding energy to the measured value and not to upset other unrelated properties.

We know that fragmentation reaction cross sections rather strongly select a neutron- $^9\text{Li}$  relative  $p$ -wave content within  $^{11}\text{Li}$  of about 40%. We also know that most of these cross sections as well as the  $^{11}\text{Li}$  binding energy and size are essentially independent of the spin-splitting because the Pauli principle for the outer neutrons requires at most one identical particle in each of these spin-split states. If one is occupied the other is as well. Then the average is the most important quantity. Thus a given  $p$ -wave content selects a one dimensional relation between the average energies of the  $s_{1/2}$  and  $p_{1/2}$  states. If the three-body potential had been known or determined from independent sources both the statistically averaged energies could have been found from  $p$ -wave content and three-body binding energy. Still an educated guess using experience provide a reasonable estimate.

We continue with spin-splitting both  $s$  and  $p$ -waves and demanding that one  $s$ -state must be at 50 keV and one  $p$ -state at 0.54 MeV. With the average positions fixed this provides the spectrum of the four  $^{10}\text{Li}$  states except that the ordering is yet undetermined and the inaccuracy from the three-body potential is also still present. Therefore we compute sensitive fragmentation data like the invariant mass spectrum which should be able to distinguish between the various  $^{10}\text{Li}$  spin assignments. Unfortunately the precision of this experimental data is not sufficient to exclude more than two of the four different, but essentially discrete, spin structures.

In conclusion, the strong connections between the properties of  $^{10}\text{Li}$  and  $^{11}\text{Li}$  are used to produce a consistent description. Experimental constraints from both nuclei are essential. We maintain the previous level of accuracy in the description of both structure and breakup reactions of  $^{11}\text{Li}$ . The spectrum of  $^{10}\text{Li}$  is confined to have average energies of  $s$  and  $p$ -states at  $0.40 \pm 0.05$  MeV. The individual  $p$ -states should appear at about 0.54 MeV (most likely the  $2^+$ -resonance) and at  $0.35 \pm 0.15$  MeV (probably the  $1^+$ -resonance). The  $s$ -states are at about 50 keV and at  $0.80 \pm 0.30$  MeV, where the present knowledge is

insufficient or too inaccurate to establish the ordering of the  $1^-/2^-$  doublet. Furthermore, the three-body potential energy, accounting for three-body polarization, off-shell effects, core-excited states beyond two-body phenomenology or other cluster configurations, must contribute by about  $0.25 \pm 0.10$  MeV to the binding energy.

**Acknowledgement.** We thank K. Riisager for continuous discussions and suggestions.

## References

- [1] M.V. Zhukov, B.V. Danilin, D.V. Fedorov, J.M. Bang, I.J. Thompson and J.S. Vaagen, Phys. Rep. **231** (1993) 151.
- [2] E. Nielsen, D.V. Fedorov, A.S. Jensen and E. Garrido, Phys. Rep. **347** (2001) 373.
- [3] K.H. Wilcox, R.B. Weisenmiller, N.A. Jelley, D. Ashery and J. Cerny, Phys. Lett. B **59** (1975) 142.
- [4] A.I. Amelin *et al.*, Sov. J. Nucl. Phys. **52** (1990) 782.
- [5] H.G. Bohlen *et al.*, Z. Phys. A **344** (1993) 381.
- [6] I. Talmi and I. Unna, Phys. Rev. Lett. **4** (1960) 469.
- [7] F.C. Barker and G.T. Hickey, J. Phys. G: Nucl. Part. Phys. **3** (1977) L23.
- [8] R.A. Kryger *et al.*, Phys. Rev. C **47** (1993) R2439.
- [9] B.M. Young *et al.*, Phys. Rev. C **49** (1994) 279.
- [10] S.N. Abramovich, B. Ya Guzhovskii and L.M. Lazarev, Phys. Part. Nucl. **26** (1995) 423.
- [11] M. Zinser *et al.*, Phys. Rev. Lett. **75** (1995) 1719.
- [12] H.G. Bohlen, W. von Oertzen, Th. Stolla, R. Kalpakchieva, B. Gebauer, M. Wilpert, Th. Wilpert, A.N. Ostrowski, S.M. Grimes and M.N. Massey, Nucl. Phys. A **616** (1997) 254c.
- [13] M. Thoennessen *et al.*, Phys. Rev. C **59** (1999) 111.
- [14] J.A. Caggiano, D. Bazin, W. Benenson, B. Davids, B.M. Sherrill, M. Steiner, J. Yurkon, A.F. Zeller and B. Blank, Phys. Rev. C **60** (1999) 064322.
- [15] M. Chartier *et al.*, Phys. Lett. B **510** (2001) 24.
- [16] F. Ajzenberg-Selove, Nucl. Phys. A **490** (1988) 1.

- [17] G. Audi and A.H. Wapstra, Nucl. Phys. A **595** (1995) 409.
- [18] Y. Tosaka and Y. Suzuki, Nucl. Phys. A **512** (1990) 46.
- [19] L. Johannsen, A.S. Jensen and P.G. Hansen, Phys. Lett. B **244** (1990) 357.
- [20] I.J. Thompson and M.V. Zhukov, Phys. Rev. C **49** (1994) 1904.
- [21] J. Wurzer and H.M. Hofmann, Z. Phys. A **354** (1996) 135.
- [22] P. Descouvemont, Nucl. Phys. A **626** (1997) 647.
- [23] F.M. Nunes, I.J. Thompson and R.C. Johnson, Nucl. Phys. A **596** (1996) 171.
- [24] N. Vinh Mau and J.C. Pacheco, Nucl. Phys. A **607** (1996) 163.
- [25] D.V. Fedorov, A.S. Jensen and K. Riisager, Phys. Rev. C **50** (1994) 2372.
- [26] E. Garrido, D.V. Fedorov and A.S. Jensen, Phys. Rev. C **53** (1996) 3159.
- [27] E. Garrido, D.V. Fedorov and A.S. Jensen, Phys. Rev. C **55** (1997) 1327.
- [28] E. Garrido, D.V. Fedorov and A.S. Jensen, Phys. Rev. C **58** (1998) R2654.
- [29] H. Simon *et al.*, Phys. Rev. Lett. **83** (1999) 496.
- [30] E. Garrido, D.V. Fedorov and A.S. Jensen, Phys. Rev. C **59** (1999) 1272.
- [31] E. Garrido, D.V. Fedorov and A.S. Jensen, Nucl. Phys. A, in press.
- [32] B.M. Young *et al.*, Phys. Rev. Lett. **71** (1993) 4124.
- [33] I. Tanihata *et al.*, Phys. Lett. B **287** (1992) 307.
- [34] J.S. Al-Khalili, J.A. Tostevin and I.J. Thompson, Phys. Rev. C **54** (1996) 1843.
- [35] P. Egelhof, ENAM2001, Proc. Int. Conf. on Exotic Nuclei and Atomic Masses, to be published.
- [36] E. Garrido, D.V. Fedorov and A.S. Jensen, Nucl. Phys. A **617** (1997) 153.
- [37] D. Baye, J. Phys. A **20** (1987) 5529.
- [38] F. Cooper, A. Khare and U. Sukhatme, Phys. Rep. **251** (1995) 267.
- [39] E. Garrido, D.V. Fedorov and A.S. Jensen, Nucl. Phys. A **650** (1999) 247.
- [40] J. Carlson and R. Schiavilla, Rev. Mod. Phys. **70** (1998) 743.
- [41] D. V. Fedorov and A. S. Jensen, Phys. Lett. B **389** (1996) 631.
- [42] A.S. Jensen, E. Garrido and D.V. Fedorov, Few-Body Systems, **22** (1997) 193.
- [43] M. Zinser *et al.*, Nucl. Phys. A **619** (1997) 151.
- [44] H. Simon, Ph.D. Thesis, Technische Universität, Darmstadt, 1998.
- [45] F. Humbert *et al.*, Phys. Lett. B **347** (1995) 198.
- [46] H. Geissel and W. Schwab, private communication.